Numerical design of a high efficiency and ultra-broadband terahertz cross-polarization converter

Materials Research Express

OPEN ACCESS

RECEIVED
11 April 2021

REVISED
19 May 2021

ACCEPTED FOR PUBLICATION
20 May 2021

PUBLISHED
2 June 2021

PAPER

Numerical design of a high efficiency and ultra-broadband terahertz cross-polarization converter

Thanh Nghia Cao[1], **Minh Tam Nguyen**[1], **Ngoc Hieu Nguyen**[1], **Chi Lam Truong**[2] and **Thi Quynh Hoa Nguyen**[1,*]

[1] School of Engineering and Technology, Vinh University, 182 Le Duan, Vinh, Vietnam
[2] NTT Hi-Tech Institute, Nguyen Tat Thanh University, Ho Chi Minh, Vietnam
[*] Author to whom any correspondence should be addressed.

E-mail: ntqhoa@vinhuni.edu.vn

Keywords: Metamaterials, Polarization Converter, Broadband, Wide-angle, Terahertz

Abstract

A simple design of terahertz polarization converter has attracted great attention owing to the applicability of terahertz technology in broad fields such as imaging, non-destructive sensing, and communications, but remains a key challenge to simultaneously achieve both wide bandwidth and high conversion efficiency. Here we report a single-layer metasurface-based polarization converter formed by a combination of different resonator shapes that realizes cross-polarization conversion and achieves an ultra-broadband and high conversion efficiency with a wide oblique incidence in the terahertz region from 1.35 THz to 3.55 THz. The high performance and physical mechanism attributed to both electric and magnetic resonances of this proposed structure are guaranteed and analyzed by numerical study. Our design structure provides the frequency tunability to other frequency bands and possesses promising applications in terahertz polarization-control devices.

1. Introduction

Terahertz technology is a fast-growing field with various potential applications in imaging, non-destructive sensing, and communications [1–5]. The terahertz wave has a frequency ranges from 0.1THz to 10THz in the electromagnetic (EM) spectrum, which in between microwave and infrared. However, the EM response of traditional materials in the terahertz range is very weak due to is non-ionizing property of terahertz radiation [6]. In recent years, metasurfaces, which are the two-dimensional equivalents of metamaterials, have drawn increasing attention for various applications because of their unique EM properties that have not been found in natural materials [7–11]. Due to unique properties, metasurfaces provide a novel way to manipulate EM waves, including their polarization conversion [12–15]. Up to now, some kinds of terahertz polarization converters (PCs), namely linear-to-linear [13, 16], linear-to-circular [17, 18], circular-to-circular [19, 20], and multifunctional [21] polarization conversion have been proposed. Among them, linear-to-linear or cross-polarization conversion has extensively studied for a wide range of applications such as in radar cross-section (RCS) and interference reduction, antenna gain enhancement, and reducing reflections during measurements [22]. The terahertz cross-polarization converter (CPC) is designed to work either in reflection or/and transmission modes. Compared to the reflection mode, the fabrication of the CPC operated in transmission mode is significantly difficult because its structure requires multilayer layers. Recently, a single layer of different asymmetry resonator shapes based on split-ring structure such as a split ring [23], double split-ring [24], double square split-ring[25], split-ring with center disk [13, 26], a combination of a single-split ring and a double-split ring[27], have been realized to design the terahertz reflective CPC. However, the main drawback of these converters is the narrow operating bandwidth or low conversion efficiency and angular tolerance. Therefore, to overcome these drawbacks, many structures based on other asymmetry metasurfaces have been proposed. For example, Lu *et al* proposed the reflective CPC base on L-shape metamaterial, which can realize a conversion efficiency higher than 98% in the terahertz range of 4.2–5.2THz, but, its relative bandwidth is still narrow below

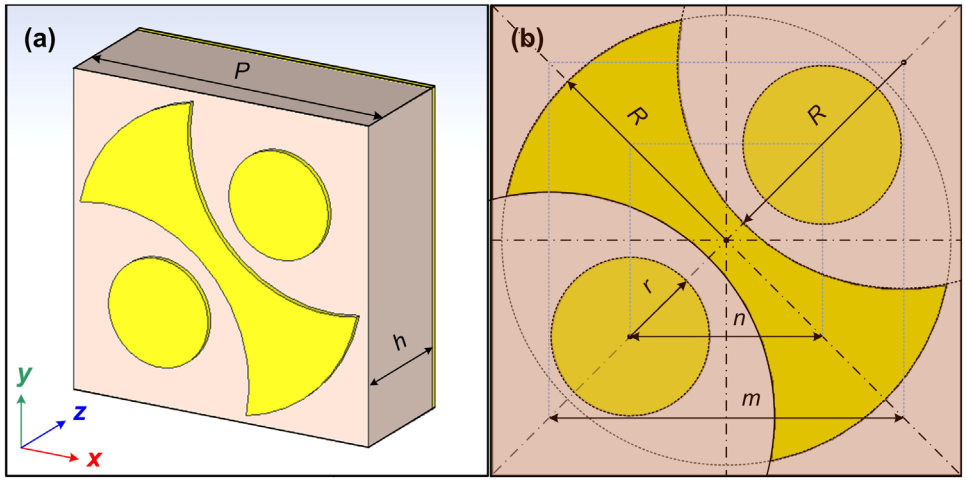

Figure 1. Geometry of the proposed converter: (a) perspective and (b) top views.

21.28 %[28]. Ako *et al* presented broadband and wide-angle CPC made of T-shape metasurface and its relative bandwidth reached to 101.54% in the range of 0.34–1.04THz, however, polarization conversion ratio (PCR) is still low than 80% [29]. Therefore, the design of terahertz reflective CPC remains a significant challenge to achieve simultaneously simple structure for fabrication, high conversion efficiency, broad bandwidth, and wide incident angle insensitivity.

Herein, we propose a simple design of high efficiency and ultra-broadband CPC using an anisotropic metasurface operating in the reflection mode in the terahertz region. The proposed CPC is composed of a periodic array of a metallic resonator formed by a combination of two disks and a double-headed axe and a dielectric substrate backed with a bottom metallic ground plane. The performance and operation principle of the proposed converter are numerically and experimentally investigated. The designed CPC shows a cross-polarization response with the relative bandwidth (RBW) of 87.68% and the polarization converter ratio (PCR) above 94% in the frequency range from 1.39 to 3.56 THz. Furthermore, this conversion efficiency is maintained with a large incident angle up to 40°. Therefore, the proposed converter should be promising for terahertz polarization-control devices.

2. Structure design and principle

The aim of this CPC design is to work in the terahertz wave that obtains a wideband and high conversion efficiency as much as possible at a wide incident angle. It means that the designed broadband CPC structure must eliminate the destructive interference that normally occurs in the middle of the operating frequency range of CPC based on meandering line with an increase in the incident angle [23, 25, 28]. To avoid this destructive interference, the design of CPC utilized the gradient structure based on crescent-shaped resonator was proposed, however, its bandwidth is still low [15]. Furthermore, the combination of some resonators was conducted to improve bandwidth of CPC [30]. Therefore, in this study, we utilize the advanced property of a gradient structure associated with arrangement of two circles to form the unit cell with its symmetry along the diagonal direction to design an efficient broadband CPC as shown in figure 1. The unit cell of the CPC consists of a metallic resonator combined by two disks and double-headed axe and a dielectric substrate backed by a metallic ground plane, as shown in figure 1(a). The dielectric substrate is made by Poly tetra fluoroethylene (PTFE) with thickness (h) of 17 μm. The PTFE substrate has a relative dielectric constant of 2.1 and a loss tangent of 0.0002. The top and the bottom layers are made by copper with an electric conductivity of 5.96×10^7 S/m and a thickness of 0.27 μm. The optimized geometrical parameters of the unit cell are given by $P = 48.6$ μm, $r = 23$ μm, $r = 8.1$ μm, $m = 18$ μm, and $n = 9.8$ μm, as shown in figure 1(b). It shoud be noted that the dimension of the unit cell is a few tens of micrometers, which can be easily fabricated by the current status of fabrication techniques such as photo-lithography.

It was recently reported that there is good agreement between CST Microwave Studio simulations and measurement results for CPC [13–15, 31]. Therefore, to investigate the conversion features of the designed CPC, the commercial computer simulation technology (CST) Microwave Studio software has been conducted using a frequency-domain solver. In the simulation setup, the unit cell boundaries are chosen for the x and y directions while the open boundary condition is applied in the z-direction. Tetrahedral mesh is used in the simulation model with an accuracy of 10^{-4} and a total number of tetrahedrons of 18,977. Because the unit cell is symmetric

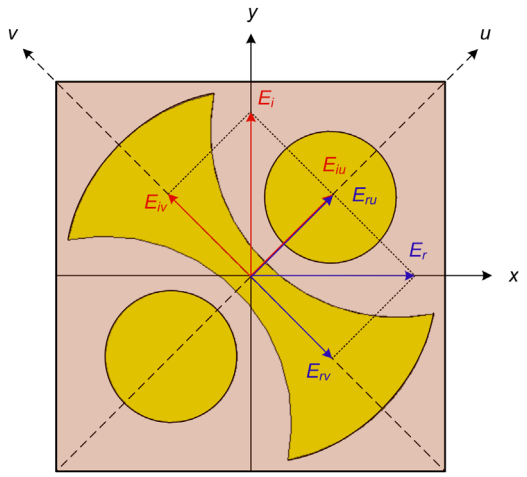

Figure 2. Decomposition of *y*-polarization incident field into *u*- and *v*-components and its conversion into *x*-polarization reflection wave.

along the diagonal direction, the coefficients of cross- and co-polarization reflection for the *y*-axis are the same as those for *x*-axis. Therefore, in this study, only *y*-polarization incident wave is considered.

The performance of polarization conversion of a CPC can be demonstrated by the polarization converter ratio (PCR), which is defined as equation (1) [31–33].

$$PCR = \frac{|r_{xy}|^2}{|r_{xy}|^2 + |r_{yy}|^2} \tag{1}$$

where, r_{xy} and r_{yy} are of the cross- and co-polarization reflection coefficients, respectively.

The working principle of the CPC is presented in figure 2. The y-polarized incident EM wave ($\boldsymbol{E}_i$) can decompose into *u*- and *v*-components. The *u*- and *v*-axes are rotated $\pm 45^\circ$ to *y*-axis, as shown in figure 2. The incident and reflection waves are given by equations (2) and (3) respectively [32].

$$\boldsymbol{E}_i = \hat{y}E_i = \hat{u}E_{iu} + \hat{v}E_{iv} \tag{2}$$

$$\boldsymbol{E}_r = \hat{u}E_{ru} + \hat{v}E_{rv} = \hat{u}\left(r_{uu}E_{iu}e^{i\Phi_{uu}} + r_{uv}E_{iv}e^{i\Phi_{uv}}\right) + \hat{v}\left(r_{vv}E_{iv}e^{i\Phi_{vv}} + r_{vu}E_{iu}e^{i\Phi_{vu}}\right) \tag{3}$$

where, $\hat{u}$ and $\hat{v}$ are the unit vectors; r_{uu}, Φ_{uu} and r_{vv}, Φ_{vv} are amplitude and phase of co-reflection coefficients for *u*-to-*u* and *v*-to-*v* polarization conversion, respectively; r_{vu}, Φ_{vu} and r_{uv}, Φ_{uv} are amplitude and phase of cross-reflection coefficients for *u*-to-*v* and *v*-to-*u* polarization conversion, respectively.

The proposed converter yields anisotropic properties with dispersive relative permittivity and permeability because of its asymmetric structure [18]. Thus, there is a difference in the phase and amplitude of reflection waves in *u*- and *v*-components. If $r_{uu} = r_{vv} \approx 1$, $r_{uv} = r_{vu} \approx 0$, and $\Delta\varphi = \Phi_{uu} - \Phi_{vv} = \pm 180^o + 2k\pi$ (k is integer), the synthetic fields of E_{ru} and E_{rv} will lie along the *x*-axis, as demonstrated in figure 2. It means that the polarized incident wave is rotated 90° and the converter reveals a cross-polarization conversion. Figure 5 shows the amplitude of reflection coefficients and phase difference ($\Delta\varphi$) for the *u*- and *v*-components. From figure 5(a), the amplitudes of the co- and cross-polarized reflection coefficients are nearly equal to 1 and 0 for the entire survey frequency range of 0.5-4.5THz, respectively. Furthermore, the phase difference between the *u*- and *v*-components is approximately $180^\circ \pm 30^\circ$ in the range of 1.29–3.66THz. It was reported that the excellent polarization conversion ratio can be obtained if a reflection phase difference is within the range of $180 + 37^\circ$ to $180–37^\circ$ [25]. Furthermore, the phase difference curve intersects the straight line with a phase of 180° at three points of 1.49 THz, 2.08 GHz, and 3.35 GHz. At these resonant points, the phase difference is equal to 180°, indicating that the designed CPC exhibits the ultra-broadband cross-polarization conversion characteristics with excellent polarization conversion efficiency.

3. Results and discussion

Figure 4 presents the amplitude and the phase difference of the reflection coefficients for the *y*-polarization incident wave under normal incidence. As seen in figure 4(a), the three resonant peaks are indexed at 1.49 THz, 2.25 THz, and 3.37 THz. At these peaks, the amplitudes of co-reflection coefficients (r_{yy}) are 0.015, 0.0047, and 0.019 and the amplitudes of cross-reflection coefficients are (r_{xy}) are 0.9797, 0.9999, and 0.9767, respectively. Moreover, the cross-polarization coefficient (r_{xy}) is kept higher than 0.95, while the co-polarization

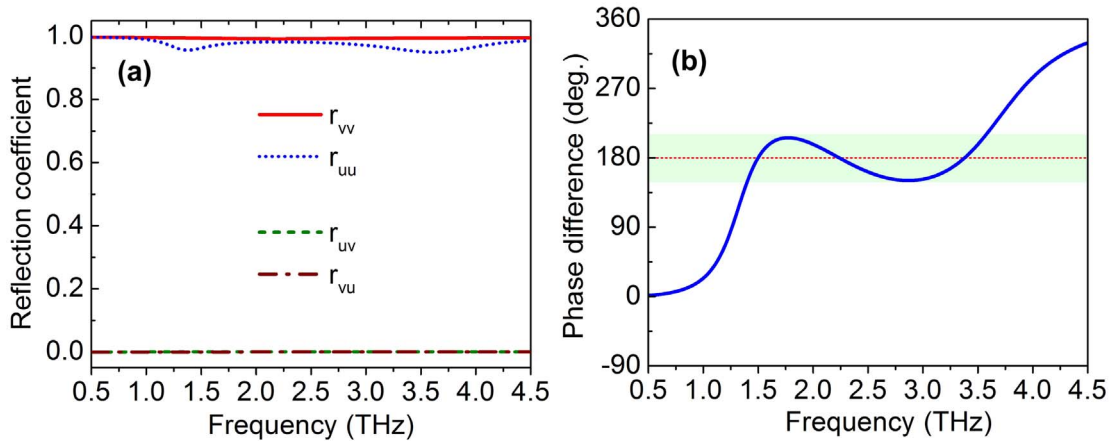

Figure 3. (a) Amplitude and (b) phase difference of the reflection coefficients of the proposed converter for *u*- and *v*-components at the normal incidence.

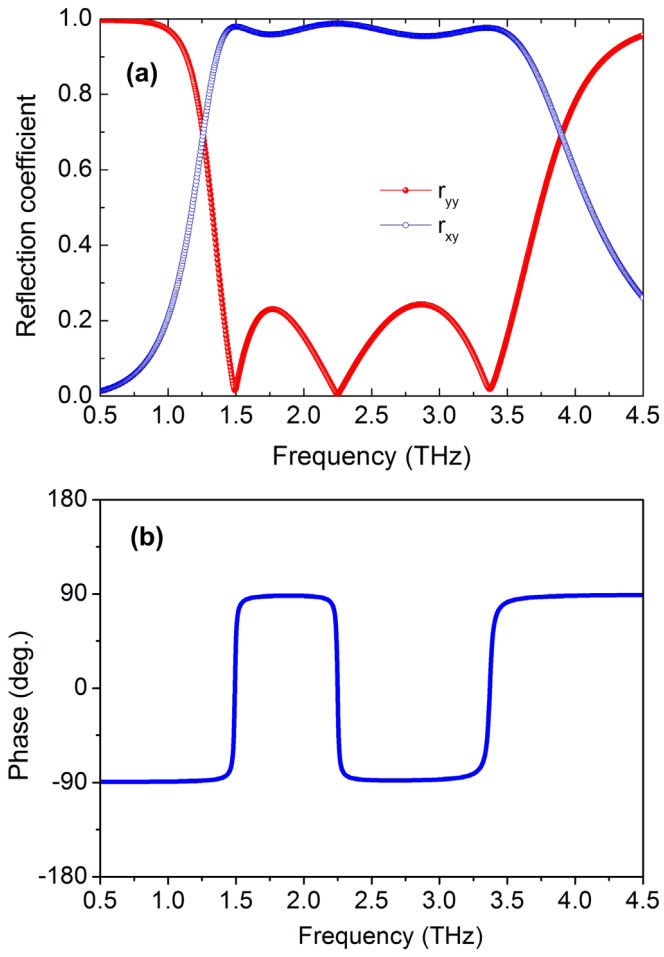

Figure 4. (a) Amplitude and (b) phase difference of cross- and co-polarized reflection coefficients of the proposed converter under normal incidence.

coefficient (r_{yy}) is maintained below 0.24 in the frequency range from 1.38 THz to 3.6 THz. The different phase of the co- and the cross-polarization coefficient is illustrated in figure 4(b). The phase difference ($\Delta\varphi$) is $\pm 90^{\circ}$ in the whole operation band. These observations are due to the fact that the perfect ultra-broadband cross-polarization conversion can occur in the proposed converter. To prove this point, the PCR curve of the proposed converter is calculated using equation (1), as depicted in figure 5. At three resonance peaks, the PCR is nearly 100%. Furthermore, the PCR is higher than 90% in the range from 1.39 THz to 3.6 THz with a relative

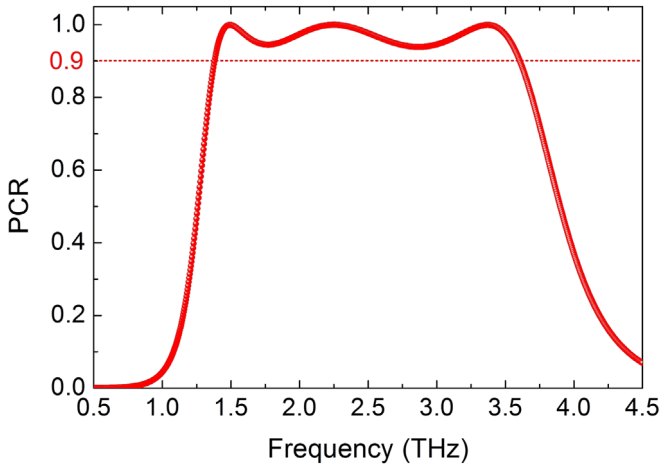

Figure 5. PCR of the proposed converter under normal incidence.

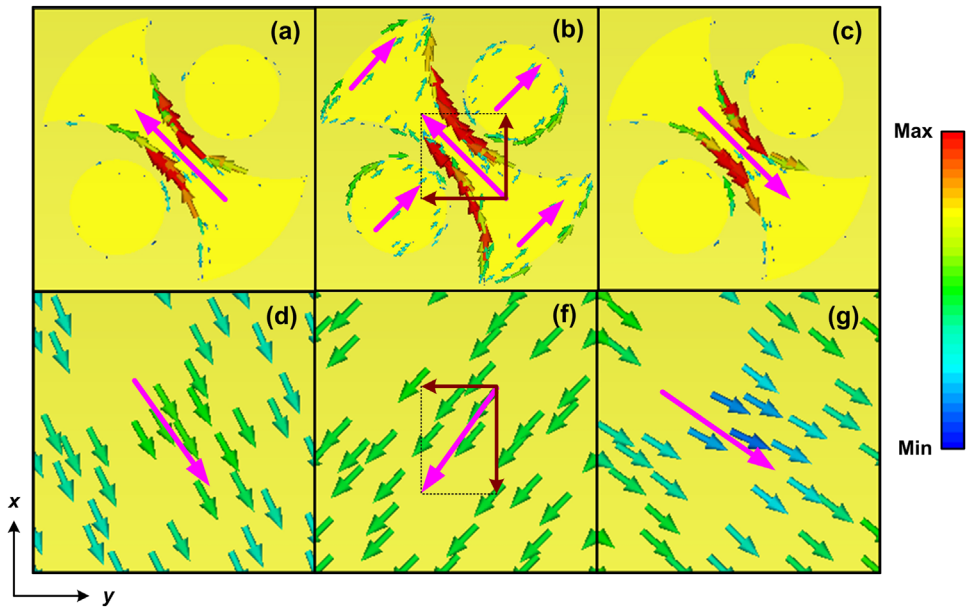

Figure 6. Surface current distributions on (a), (b), (c) the top layer and (d), (f), (g) bottom layer of the proposed CPC at various frequencies of 1.49 THz, 2.08 THz, and 3.35 THz, respectively.

bandwidth of 89.15%. it is evident that the proposed CPC can effectively work as an ultra-broadband cross-polarization converter. With an optimal region from 1.39 THz to 3.56 THz corresponding relative bandwidth of 87.68%, the PCR above 94% is achieved. The ultra-broadband conversion response mainly originates from the superposition of multiple resonance modes, corresponding to the three peaks at 1.49 THz, 2.25 THz, and 3.37 THz [13, 30].

We demonstrate the physical mechanism of the designed CPC by analyzing the distributions of surface current on the top and bottom layer at different resonant frequencies of 1.49 THz, 2.08 THz, and 3.35 THz, as presented in figure 6. At the lower frequencies of 1.49 THz, the top surface current is anti-parallel with the bottom surface current, revealing the magnetic resonance contributes to this resonant frequency [25, 27, 30]. In contrast, at a higher frequency of 3.35GHz, the surface current distributions on the top and bottom layers are parallel, which is produced by electric resonance [25, 27, 30]. Meanwhile, at the resonant frequency of 2.08 THz, the direction of the top surface current is different. The minor component of surface current on the top layer is anti-parallel with the bottom surface current. The main component of surface current on the top layer is along the axe resonator that can be synthesized into two components in the x- and *y*-axis directions, where the top surface current in the *x*-axis direction is anti-parallel with the synthesized bottom surface current in the *x*-axis direction and the top surface current in the *y*-axis direction is parallel with the synthesized bottom surface

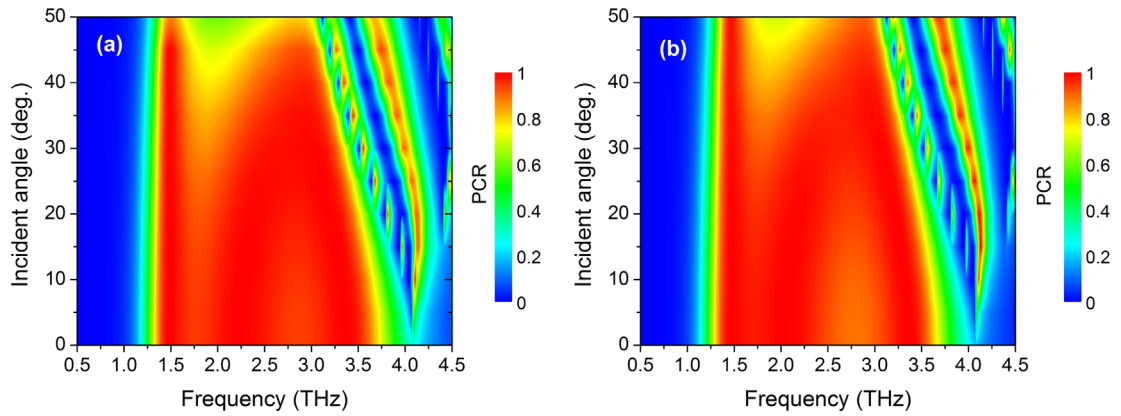

Figure 7. The PCR map of the proposed polarization converter as a function of the frequency and the incident angle for (a) TE and (b) TM polarizations.

current in the *y*-axis direction as shown in figures 6 (b) and (f). It means that the resonant frequency of 2.08 THz is due to magnetic resonance associated with the electric resonance.

An important key of CPC design is that the CPC can work with large incident angles to suitable for practical applications. Thus, we introduce the simulated dependence of the PCR on the incident angles in the range of 0–50° for both transverse electric (TE) and transverse magnetic (TM) polarizations, as depicted in figures 7(a) and (b), respectively. The bandwidth of the proposed CPC s hrinks with increasing for both polarizations, which is owing to the destructive interference at the surface of the metasurface structure with large incident angles [30]. However, the PCR value persists as high as 80% in the operating frequency range from 1.38THz to 3.11THz with a relative bandwidth of 77.06%, when the incident angle changes from 0° to 40°. This demonstrates the wide-angle insensitive cross-polarization conversion behavior of the designed structure.

We also assess the effect on the performance of the proposed structure for the different unit cell dimensions. Figure 8 shows the simulated amplitude of co- and cross-polarization reflection coefficients, phase difference, and PCR as a function of the scaling of unit cell dimension in the range of 0.5 to 1.5 with a step of 0.25. As shown in figure 8, the operating frequency is shifted to the higher frequency range by decreasing the scaling of the unit cell dimension from 1.5 to 0.5. Meanwhile, with varying the scaling in the range from 0.5 to 1.5, the amplitude of co- and cross-polarization reflections and their phase difference are almost unchanged in its operating frequency. The detailed operating frequency range and the corresponding relative bandwidth of the proposed structure with varying the scaling of unit cell dimensions are presented in table 1. The value of scaling has a great effect on operating frequency range, but the relative bandwidth is kept nearly constant, as indicated in table 1. These results indicate that the proposed CPC structure can be used to design the ultra-broadband polarization converter operating in suitable frequency regimes for practical applications by tailoring the unit cell dimension scaling.

Finally, we have compared the performance of our designed CPC with other recently reported broadband PCs in the terahertz regime. Table 2 shows the converter properties in terms of operating frequency, PCR, relative bandwidth, and *destructive interference with an increase in the incident angle*. It can be seen from 2, the proposed converter has excellent performance, characterized by high conversion efficiency, wide relative bandwidth, simultaneously. As compared to the CPC in [29], our design exhibits a smaller RBW but a higher PCR. Meanwhile, our design shows a lower PCR but a much higher RBW when compared to the CPCs in [23, 28]. In addition, comparing with the CPC in [25], our design shows the same RBW and PCR values, but destructive interference with an increase in the incident angle, indicating that it has a superior property of the wide-angle insensitivity.

4. Conclusion

We have proposed a single-layer metasurface-based PC that comprises different resonator shapes of two disks and a double-headed axe for the terahertz region. The performance and conversion mechanism were numerically analyzed. The simulated results show that the designed PC reveals a cross-polarization converter behavior in the wide frequency range of 1.39–3.56 THz with a high PCR above 94% and wide-angle insensitivity up to 40°. The designed structure can be extended to work in other operation frequencies by scaling its dimension. The excellent performance and frequency tunability of the designed PC structure demonstrates applicability to terahertz polarization-control devices.

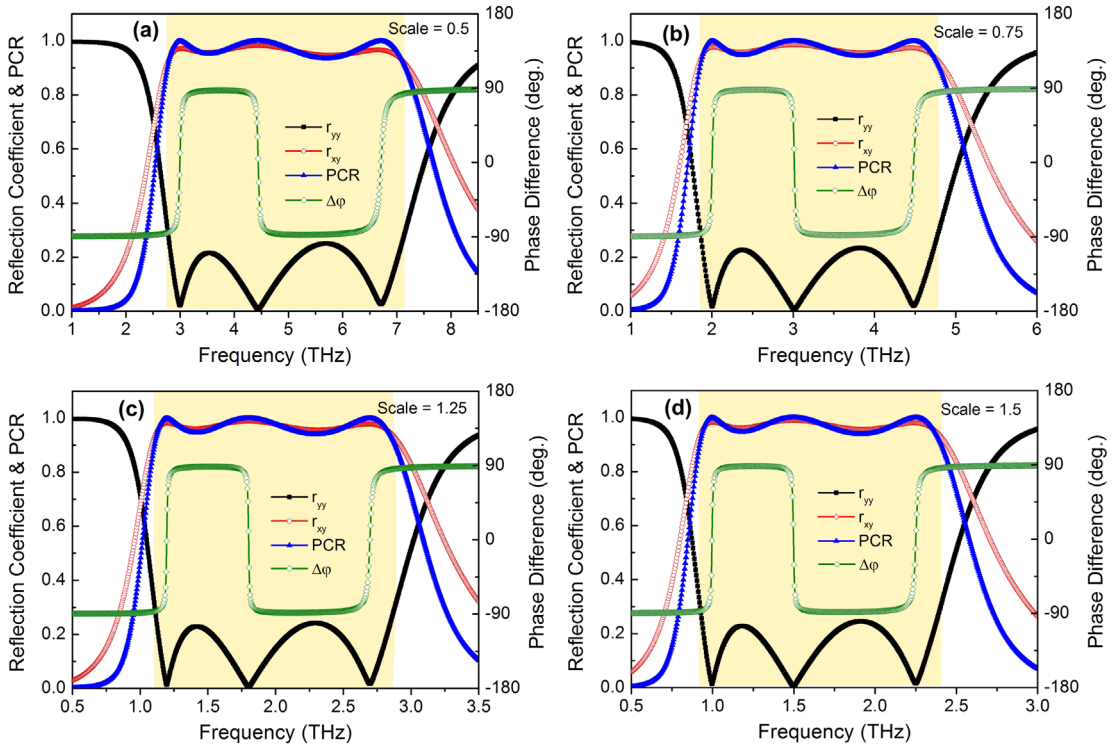

Figure 8. (a) Amplitude and (b) phase difference of co- and cross-polarized reflection coefficients of the proposed polarization under normal incidence.

Table 1. The performance of the proposed CPC structure with various the scaling of the unit cell dimension.

Scale	Operating band with PCR > 90% (THz)	RBW with PCR > 90% (%)
0.5	2.75-7.17	89.10
0.75	1.84-4.8	89.15
1.0	1.38-3.6	89.16
1.25	1.1-2.87	89.16
1.5	0.92-2.4	89.15

Table 2. Performance comparison of the designed CPC with other broadband polarization converter.

Reference	Operating band (THz)	PCR	RBW (%)	Destructive interference with an increase in the incident angle
[13]	0.65-1.45	0.8	76.6	Yes
[33]	0.41-0.96	0.8	80.3	NA
[26]	0.65-1.58	0.8	83.41	NA
[29]	0.34-1.04	0.8	101.54	No
[25]	2.04-5.33	0.9	89	Yes
[28]	4.2-5.2	0.98	21.28	Yes
[23]	2.98-4.16	0.98	33.05	Yes
This work	1.39-3.56	0.94	87.68	No
	1.39-3.6	0.9	89.15	

Acknowledgments

This research is supported by Vietnam National Foundation for Science and Technology Development (NAFOSTED) under grant number 8/2020/STS02.

Data availability statement

All data that support the findings of this study are included within the article (and any supplementary files).

Conflict of Interest

The authors declare no conflict of interest.

ORCID iDs

Thi Quynh Hoa Nguyen https://orcid.org/0000-0002-0955-8241

References

[1] Ferguson B and Zhang X-C 2002 *Nat. Mater.* **1** 26
[2] Guerboukha H, Nallappan K and Skorobogatiy M 2018 *Adv. Opt. Photonics* **10** 843
[3] Taylor Z D *et al* 2011 *IEEE Trans. Terahertz Sci. Technol.* **1** 201
[4] Huang Z, Park H, Parrott E P J, Chan H P and Pickwell-MacPherson E 2013 *IEEE Photonics Technol. Lett.* **25** 81
[5] Nagatsuma T, Ducournau G and Renaud C C 2016 *Nat. Photonics* **10** 371
[6] Wallace V P, Macpherson E, Zeitler J A and Reid C 2008 *J. Opt. Soc. Am.* A **25** 3120
[7] Pendry J B 2000 *Phys. Rev. Lett.* **85** 3966
[8] Liang D, Gu J, Han J, Yang Y, Zhang S and Zhang W 2012 *Adv. Mater.* **24** 916
[9] Tao H, Landy N I, Bingham C M, Zhang X, Averitt R D and Padilla W J 2008 *Opt. Express* **16** 7181
[10] Tuan T S and Hoa N T Q 2019 *IEEE Photonics J.* **11** 18648698
[11] Holloway C L, Kuester E F, Gordon J A, O'Hara J, Booth J and Smith D R 2012 *IEEE Antennas and Propag.* **54** 10
[12] Grady N K, Heyes J E, Chowdhury D R, Zeng Y, Reiten M T, Azad A K, Taylor A J, Dalvit D A and Chen H-T 2013 *Science* **340** 1304
[13] Cheng Y Z, Withayachumnankul W, Upadhyay A, Headland D, Nie Y, Gong R Z, Bhaskaran M, Sriram S and Abbott D 2014 *Appl. Phys. Lett.* **105** 181111
[14] Nguyen T K T, Nguyen T M, Nguyen H Q, Cao T N, Le D T, Bui X K, Bui S T, Truong C L, Vu D L and Nguyen T Q H 2021 *Sci. Rep.* **11** 2032
[15] Nguyen T Q H, Nguyen T K T, Nguyen T Q M, Cao T N, Phan H L, Luong N M, Le D T, Bui X K, Truong C L and Vu D L 2021 *Opt. Commun.* **468** 126773
[16] Liu W, Chen S, Li Z, Cheng H, Yu P, Li J and Tian J 2015 *Opt. Lett.* **40** 3185
[17] Jiang Y, Wang L, Wang J, Akwuruoha C N and Cao W 2017 *Optics Express.* **25** 27616
[18] Jiang Y, Zhao H, Wang L, Wang J, Cao W and Wang Y 2019 *Opt. Mater. Express* **9** 2088
[19] Jia M *et al* 2019 *Light Sci. Appl.* **8** 16
[20] Cheng Y, Fan J, Luo H, Chen F, Feng N, Mao X and Gong R 2019 *Opt. Mater. Express* **9** 1365
[21] Jiang H, Zhao W and Jiang Y 2017 *Opt. Mater. Express* **7** 4277
[22] Ako R T, Lee W S L, Atakaramians S, Bhaskaran M, Sriram S and Withayachumnankul W 2020 *APL Photon.* **5** 046101
[23] Yang X, Zhang B and Shen J 2018 *Opt. Quant. Electron.* **50** 315
[24] Wen X and Zheng J 2014 *Opt. Express* **22** 28292
[25] Qi Y, Zhang B, Liu C and Deng X 2020 *IEEE Access* **8** 116675
[26] Zhao J, Cheng Y and Cheng Z 2018 *IEEE Photonics J.* **10** 4600210
[27] Wu P, Da-jun S and Yan-jun Y 2018 *Optoelectron. Lett.* **14** 434
[28] Lu T, Qiu P, Lian J, Zhang D and Zhuang S 2019 *Opt. Mater.* **95** 109230
[29] Ako R T, Lee W S L, Bhaskaran M, Sriram S and Withayachumnanku W 2019 *APL Photon.* **4** 096104
[30] Xu J, Li R, Qin J, Wang S and Han T 2018 *Opt. Express* **26** 20913
[31] Hao J, Yuan Y, Ran L, Jiang T, Kong J A, Chan C T and Zhou L 2007 *Phys. Rev. Lett.* **99** 063908
[32] Khan M I, Khalid Z and Tahir F A 2019 *Sci. Rep.* **9** 4552
[33] Ma S, Wang X, Luo W, Sun S, Zhang Y, He Q and Zhou L 2017 *Epl-europhys. Lett.* **117** 37007